RSC Advances

ROYAL SOCIETY OF CHEMISTRY

www.rsc.org/advances

Journal Name

RSCPublishing

ARTICLE

Upconversion assisted BiOI/$ZnWO_4$: Er^{3+}, Tm^{3+}, Yb^{3+} heterostructures with enhanced visible and near-infrared photocatalytic activities

Cite this: DOI: 10.1039/xoxxooooox

Received ooth January 2012,
Accepted ooth January 2012

DOI: 10.1039/xoxxooooox

www.rsc.org/

Shouqiang Huang,[a] Yingming Feng,[b] Lihua Han,[b] Ziyang Lou,[a] Zhibin Qi,[a] Bao Yu[a] and Nanwen Zhu*[a]

Photocatalytic activities of near-infrared (NIR) photocatalysts can be improved by the formation of heterostructures, and an efficient semiconductor upconversion agent of $ZnWO_4$: Er^{3+}, Tm^{3+}, Yb^{3+} (ZWOETY) was applied to synthesize the BiOI/ZWOETY (BOI/ZWOETY) composite with p-n heterostructure. BOI/ZWOETY displays the flower-like structure, and ZWOETY nanoparticles are found to be dispersed homogeneously throughout the BOI surfaces, which is beneficial for the NIR light harvesting. Due to the upconversion luminescence property of ZWOETY, NIR light can be upconverted to a wide range of light emissions, including the red (658 nm), green (526 and 550 nm), blue (483 nm), violet (410 nm), and UV (367 and 380 nm) light, and all these upconversion emissions can be absorbed by BOI for photocatalysis. Under visible and NIR light irradiations, BOI/ZWOETY all shows better photocatalytic activities in degradation of methyl orange (MO) and salicylic acid (SA), compared to pure BOI and BOI/ZWO. The generation of holes contributes to the MO and SA decomposition greatly, and the upconversion properties and the highly efficient separation of electron-hole pairs are responsible for the enhanced photocatalytic activities in BOI/ZWOETY.

Introduction

The development of visible and near-infrared (NIR) light photocatalysts is critical for the efficient sunlight harvesting and the improvement of photocatalytic activities. The visible light photocatalysts, i. e., the metallic or nonmetallic elements doped TiO_2,[1] Bi-based oxides,[2] and sulfur compounds,[3] have been widely studied, while the research efforts on the NIR photocatalysts are still needed to improve the NIR-driven photocatalytic activities. The incorporated semiconductor photocatalysts with upconversion materials can increase the NIR driven photocatalytic activities, and open a door for the potential full-spectrum utilization of solar energy.[4-8] Up to now, the upconversion materials involved mainly focus on the fluoride agents owing to their high upconversion emission efficiencies, while the physicochemical stabilities of fluorides are really lower compared to metal oxides,[9] and the heterostructure properties are rarely present in the NIR photocatalysts with fluoride/metal oxide structures. $ZnWO_4$ has been proven as a promising upconversion host material for lanthanides, due to its low crystal symmetrical monoclinic wolframite structure and low phonon energies.[10-12] As an n-type semiconductor with large band gap energy, $ZnWO_4$ has been also widely used for heterogeneous photocatalysis.[13,14] Thus, the NIR photocatalyst, coupled with the semiconductor upconversion agent of lanthanides doped $ZnWO_4$, might be a good alternative for the improvement of photocatalytic activities.

The formation of heterostructure between $ZnWO_4$ and other semiconductor will greatly enhance the electron-hole pair separation in the NIR photocatalyst systems. BiOI is a typical p-type semiconductor with efficient visible light photocatalytic activity.[15] According to the small band gap (1.69-1.92 eV) of BiOI,[16,17] most of the light emissions, including the red, green, blue, violet, and UV light upconverted through the upconversion luminescence agents from NIR light,[6,7] can be absorbed by BiOI for photocatalysis. As a consequence, the NIR photocatalyst constructed by BiOI and lanthanides doped $ZnWO_4$ will provide higher harvest efficiency of sunlight compared to pure-$ZnWO_4$/BiOI composites.[13]

In this work, a novel heterostructured NIR photocatalyst of BiOI/$ZnWO_4$: Er^{3+}, Tm^{3+}, Yb^{3+} (BOI/ZWOETY) was prepared via a simple chemical precipitation method. ZWOETY is the n-type semiconductor upconversion agent, and BOI is the p-type visible light photocatalyst in the BOI/ZWOETY composite. Besides the utilization of UV and visible light directly by BOI, the NIR light will be upconverted to the additional visible and UV light by ZWOETY, which enable to excite BOI for the enhancement of photoactivity. The structures, morphologies and upconversion properties of the samples were characterized, and the photocatalytic activities were evaluated on the degradation of methyl orange (MO) and salicylic acid (SA) under visible and NIR light irradiation. The degradation

mechanism of the enhanced photocatalytic activities was discussed based on the effects of upconversion and heterostructure properties in the BOI/ZWOETY system.

Experimental Section

Chemicals and materials

$ZnSO_4 \cdot 7H_2O$, $Na_2WO_4 \cdot 2H_2O$, $Er(NO_3)_3 \cdot 5H_2O$, $Tm(NO_3)_3 \cdot 5H_2O$, $Yb(NO_3)_3 \cdot 5H_2O$, $Bi(NO_3)_3 \cdot 5H_2O$, KI were all purchased from Sinopharm chemical Reagent Co. Ltd (China). All the chemical reagents were of analytical grade and used as received.

Preparation of ZWOETY nanoparticles

$ZnSO_4 \cdot 7H_2O$ (18 mmol), $Er(NO_3)_3 \cdot 5H_2O$ (0.09 mmol), $Tm(NO_3)_3 \cdot 5H_2O$ (0.09 mmol), and $Yb(NO_3)_3 \cdot 5H_2O$ (0.9 mmol) were dissolved into a three-necked flask containing 200 mL of distilled water with continuous mechanical stirring. 20 mmol of $Na_2WO_4 \cdot 2H_2O$ was dissolved into 40 mL distilled water, and added drop by drop into the above solution. The resulted mixture was kept at 80 ºC under stirring of 200 rpm for 6 h. The precipitates were filtered, washed with distilled water and ethanol, and then dried at 60 °C for 12h. The obtained white powders were finally heated at 500 °C for 4 h to form the ZWOETY products. Meanwhile, pure ZWO was prepared under the same condition.

Preparation of the BOI/ZWOETY composites

In a typical procedure for BOI/ZWOETY, 5 mmol of $Bi(NO_3)_3 \cdot 5H_2O$ and ZWOETY nanoparticles (mass ratio of BOI: ZWOETY is 100: 10) were added into a three-necked flask containing 100 mL of absolute ethanol and totally dispersed by ultrasonication. Then 100 mL of KI aqueous solution (0.06 M) was dropped into the above mixture with continuous mechanical stirring, and kept at 80 ºC under stirring of 200 rpm for 6 h. The BOI/ZWOETY precipitates were obtained after centrifugation and washing, and dried at 60 °C for 12 h. For comparison purposes, pure BOI, BOI/10%ZWO, BOI/30%ZWOETY, BOI/50%ZWOETY and BOI/70%ZWOETY were also synthesized with the same procedures mentioned above.

Characterization

The X-ray diffraction (XRD) patterns were measured in a Bruker D8 Advance X-ray Polycrystaline Diffractometer with Cu K_α radiation (λ=1.5406 Å), and the average crystal sizes were determined through the Scherrer formula.[4] The morphologies and microstructures were recorded with Sirion 200 field emission scanning electron microscopy (FESEM) equipped with the INCA X-Act energy-dispersive spectroscopy (EDS) instrument and JEM-2100F transmission electron microscopy (TEM). X-ray photoelectron spectroscopy (XPS) measurements were performed on a Kratos Axis UltraDLD spectrometer with a monochromatic Al K_α source (1486.6 eV), and C 1s peak (284.8 eV) was used to calibrate all the binding energies of the elements. UV-Vis-NIR (Ultraviolet-Visible-Near Infrared) diffuse reflectance spectra were obtained using the Lambda 750 UV/Vis/NIR spectrophotometer. Room temperature upconversion fluorescence spectra were measured on a Hitachi F-7000 fluorescence spectrophotometer equipped with a 980 nm semiconductor solid laser excitation.

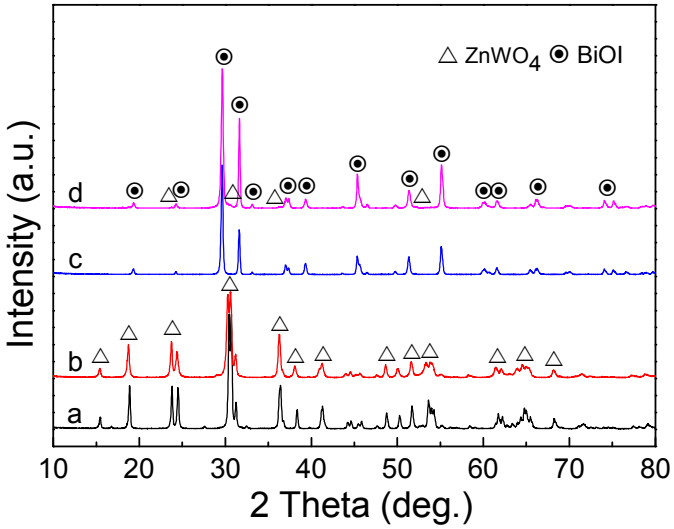

Fig. 1 Typical XRD patterns of (a) pure ZWO, (b) ZWOETY, (c) pure BOI, and (d) BOI/ZWOETY.

Photoluminescence (PL) spectra were also recorded on the Hitachi F-7000 fluorescence spectrophotometer with a 150 W xenon lamp.

Photocatalytic activities

MO degradation experiments were used to assess the photocatalytic activities of the samples under irradiations by 980 nm NIR light, and visible-NIR (Vis-NIR) light ($\lambda \geq 400$ nm) provided by a 1000 W high pressure mercury lamp or a 500 W Xe lamp. 40 mg of the samples were dispersed in MO aqueous solutions (10 ppm, 40 mL). Prior to irradiation, the resulted mixtures were kept in the dark with magnetically stirring for 2 h to ensure the adsorption/desorption equilibrium. At 30 min intervals, 2.0 mL of the suspensions were taken out following centrifugation (12000 rpm, 10 min). The concentrations of MO were measured by a UV-Vis spectrophometer (Hitachi U-3900) and the absorption peaks at 464 nm were recorded. The photocatalytic degradation experiments of SA were similar to the procedures mentioned above, and the absorption peaks at 295 nm were recorded. The photocatalytic mechanisms in MO and SA solutions were elucidated by the addition of 1.0 mM ammonium oxalate (AO), isopropyl alcohol (IPA), and benzoquinone (BQ), which were used as scavengers for holes (h^+), hydroxyl radicals (•OH), and superoxide radicals ($O_2^{\bullet-}$),[18,19] respectively. Furthermore, Terephthalic acid (TA, 4×10^{-4} M in a 2×10^{-3} M NaOH) and Nitroblue tetrazolium (NBT, 1×10^{-3} M) solutions were used to detect the •OH and $O_2^{\bullet-}$ radicals generated from the samples,[6,20] respectively, and the test methods were similar to procedures mentioned for photodegradation of MO.

Results and discussion

XRD analysis

The crystal structures of pure ZWO, ZWOETY, pure BOI, and BOI/ZWOETY are investigated by XRD (Fig. 1). The XRD pattern of pure ZWO is in good accordance with the monoclinic wolframite structure (JCPDS card no. 89-0447) (Fig. 1a). After doping with $Er^{3+}/Tm^{3+}/Yb^{3+}$ ions, the diffraction peak intensities of ZWOETY decrease slightly (Fig. 1b), and the main diffraction peaks at 18.76º, 23.74º, and 30.60º match well with the (100), (011), and (111) planes of ZWOETY (JCPDS

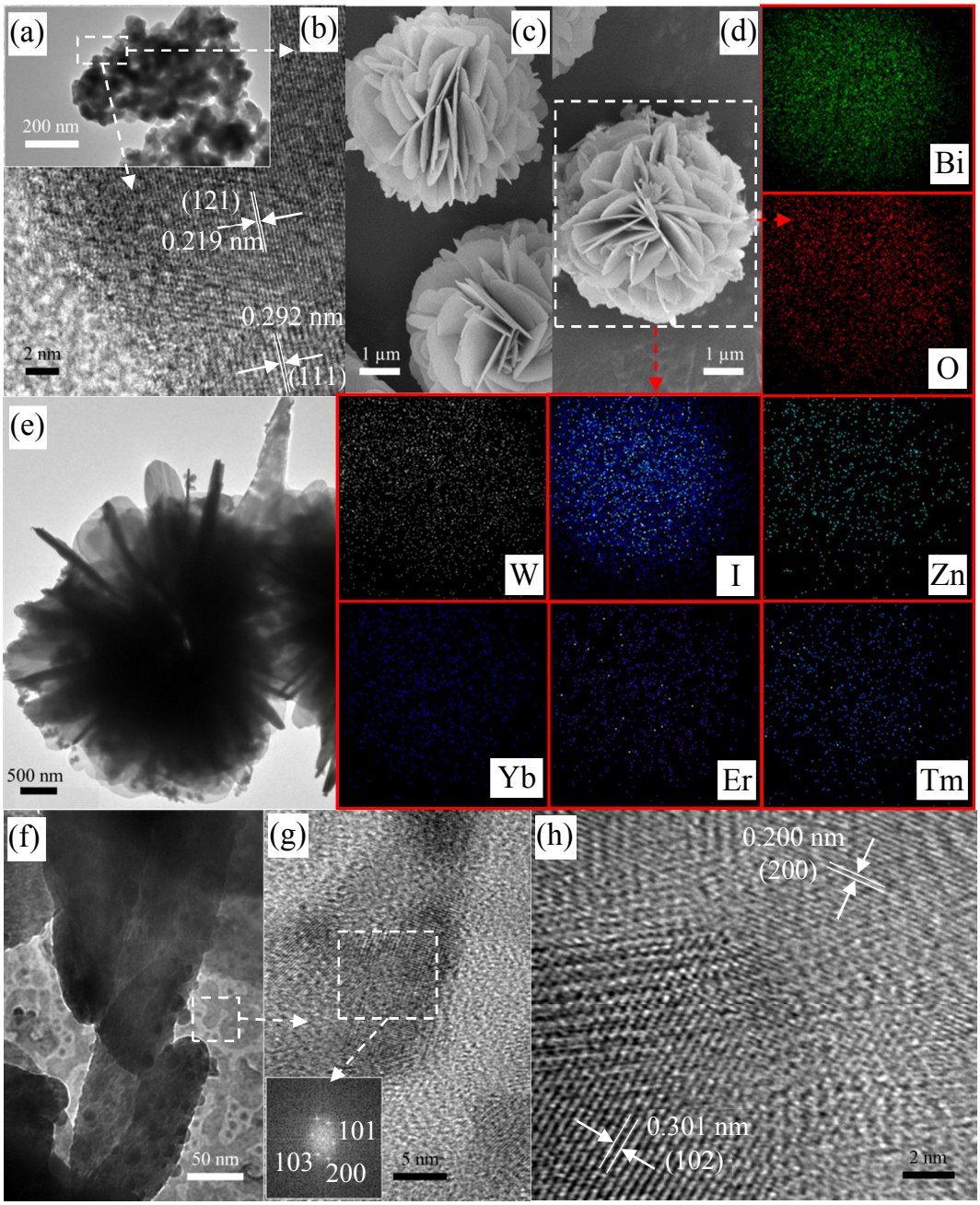

Fig. 2 (a) TEM and (b) HRTEM images of ZWOETY. SEM images of (c) pure BOI and (d) BOI/ZWOETY and its corresponding elemental distribution mapping results for Bi, O, I, Zn, W, Yb, Er, and Tm. (e, f) TEM and (g, h) HRTEM images of BOI/ZWOETY (inset: Fourier transform electron diffraction pattern).

card no. 88-0251), respectively. The average crystal size of ZWOETY is decreased to 15.69 nm compared to that (25.28 nm) of ZWO. The XRD pattern of pure BOI is attributed to the tetragonal phase of BOI (JCPDS card no. 10-0445) (Fig. 1c). For BOI/ZWOETY (Fig. 1d), the main diffraction peaks at 29.66º, 31.64º, 45.36º, 51.36º, and 55.14º are well indexed to the (102), (110), (200), (114), and (212) planes of BOI (JCPDS card no. 73-2062), and there are also present some weak diffraction peaks of ZWOETY, while these diffraction peak intensities enhanced gradually as ZWOETY added increased from 10% to 70% (Fig. S1†).

Morphology investigations

The surface morphologies of the samples are observed by SEM and TEM. Fig. 2a shows the overall morphology of ZWOETY consists of many nanoparticles, and the corresponding lattice spacings of 0.292 and 0.219 nm meet the (111) and (121) planes of ZWO (Fig. 2b). It can be seen from Fig. 2c that pure BOI possesses flower-like structure with a diameter of about 4.5 μm, which is self-assembled by flake-like BOI petals with smooth surfaces. In the case of BOI/ZWOETY, the surfaces of the BOI petals are loaded with ZWOETY nanoparticles (Fig. 2d-f). The high-resolution TEM (HRTEM) image confirms the

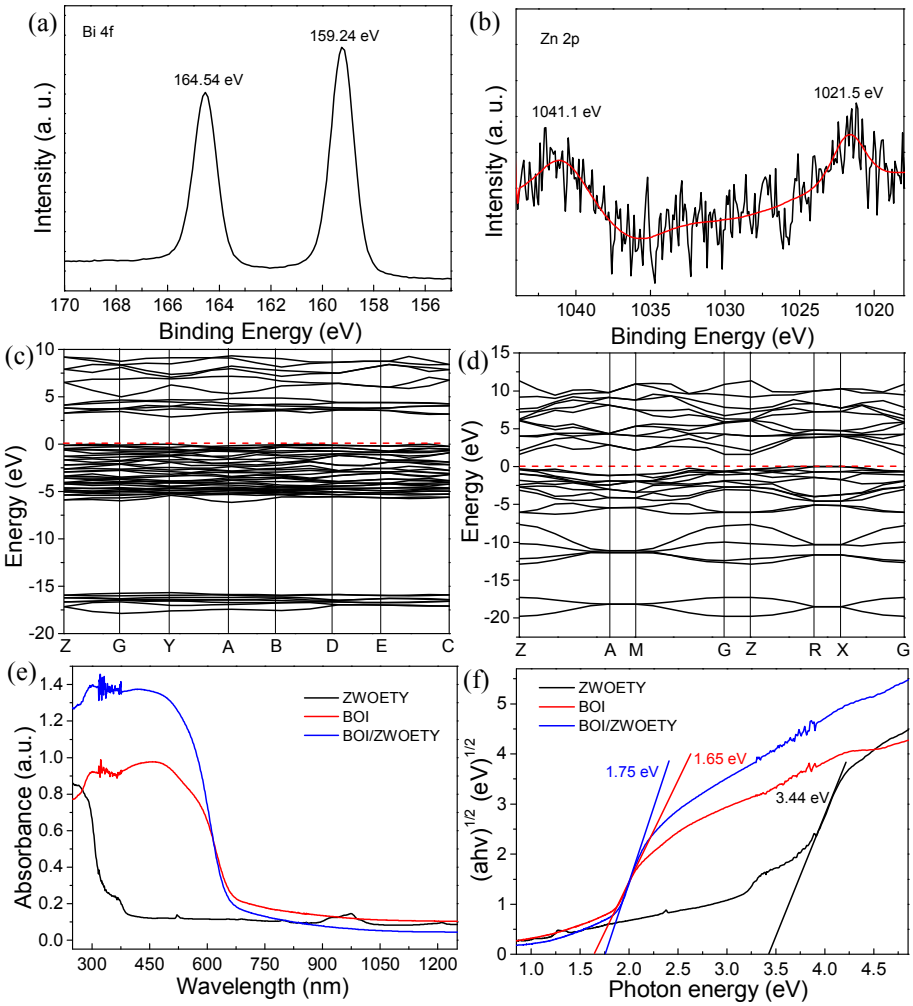

Fig. 3 XPS spectra of BOI/ZWOETY: (a) Bi 4f, and (b) Zn 2p. Band structures of (c) ZWOETY and (d) pure BOI. (c) UV-Vis-NIR diffuse reflectance spectra of ZWOETY, pure BOI, and BOI/ZWOETY. (d) Plots of the $(\alpha h\nu)^{1/2}$ versus photon energy ($h\nu$) for ZWOETY, pure BOI, and BOI/ZWOETY.

well crystallization properties of BOI/ZWOETY (Fig. 2g and h), where the lattice spacings of 0.301 and 0.200 nm are assigned to the (102) and (200) planes of BOI, and the Fourier transform electron diffraction pattern presents the preferential [010] growth direction (inset of Fig. 2g).

The EDS spectra of ZWOETY and pure BOI are shown in Fig. S2†, and the elemental mapping results of BOI/ZWOETY are highlighted by the red frames in Fig. 2. The elements Bi, O, I, Zn, W, Yb, Er, and Tm are detected with the atomic ratio of 12.36: 73.83: 11.33: 1.18: 1.14: 0.12: 0.02: 0.02 (Table S1†), respectively, and they distributed homogeneously throughout the flower-like structure (Fig. 2d). The surface elements of BOI/ZWOETY are further detected by XPS, as shown in Fig. 3a and b. The Bi 4f spectrum consists of the Bi $4f_{5/2}$ and Bi $4f_{7/2}$ peaks, which locate at 159.24 and 164.54 eV, respectively. The binding energies at 1021.5 and 1041.1 eV are attributed to Zn $2p_{3/2}$ and Zn $2p_{1/2}$, respectively. Taking the morphologies and element analytical results into account, most of the ZWOETY nanoparticles are deposited on the BOI surfaces, which is beneficial for the light harvesting and the photocatalytic reactions.

UV-Vis-NIR absorption properties

The band structures of ZWOETY (Fig. 3c) and pure BOI (Fig. 3d) are calculated using the CASTEP program package through the plane-wave density function theory (DFT), and both of them exhibit the indirect gap semiconductor property. The band gaps of ZWOETY and pure BOI are estimated to be 2.89 and 1.62 eV, respectively, while the band gaps calculated by DFT simulations are often smaller than those obtained experimentally due to the intrinsic factor of DFT.[21,22] The optical properties of the samples are examined by the UV-Vis-NIR diffuse reflectance spectra, as shown in Fig. 3e. ZWOETY exhibits absorbance in the UV light range, while two other obvious absorption peaks are found at 521 and 974 nm, which match with the $^2H_{11/2}\rightarrow{}^4I_{15/2}$ and $^4I_{11/2}\rightarrow{}^4I_{15/2}$ transitions of Er^{3+} ions, respectively. The absorption at 974 nm is also contributed by the $^2F_{5/2}\rightarrow{}^2F_{7/2}$ transitions of Yb^{3+} ions.[7] With the incorporation of BOI, BOI/ZWOETY has much stronger absorption intensity in both the UV and visible light regions, compared to pure BOI and other BOI/ZWOETY composites with ZWOETY contents of 30%, 50%, and 70% (Fig. S3†),

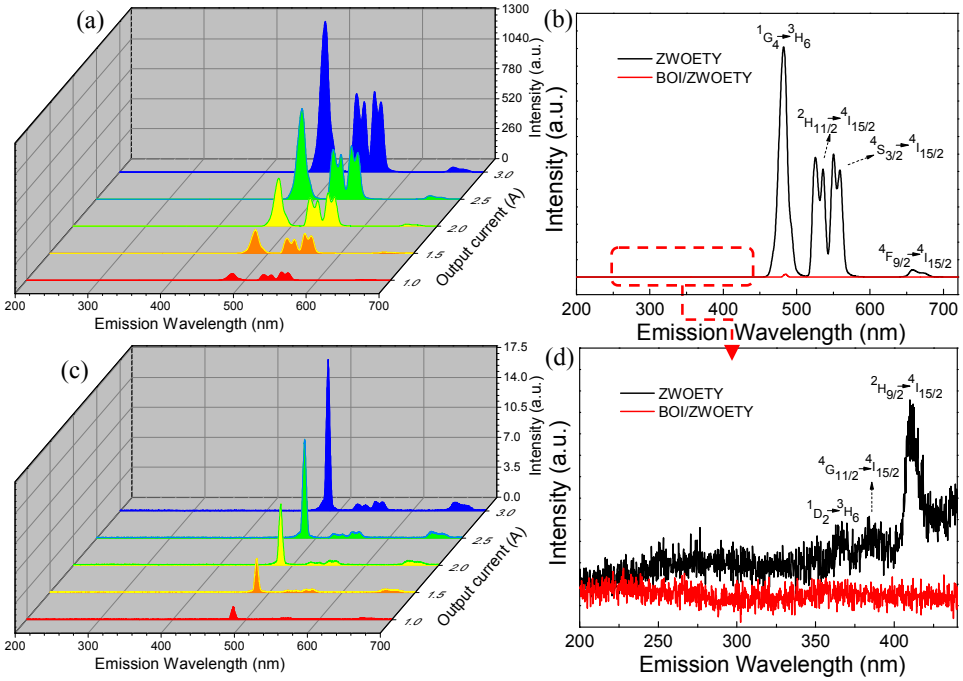

Fig. 4 Upconversion luminescence spectra of (a) ZWOETY and (c) BOI/ZWOETY under 980 nm NIR excitation with different laser output currents (1.0-3.0 A). (b, d) Upconversion luminescence spectra of ZWOETY and BOI/ZWOETY under 980 nm NIR excitation (output current = 3.0 A).

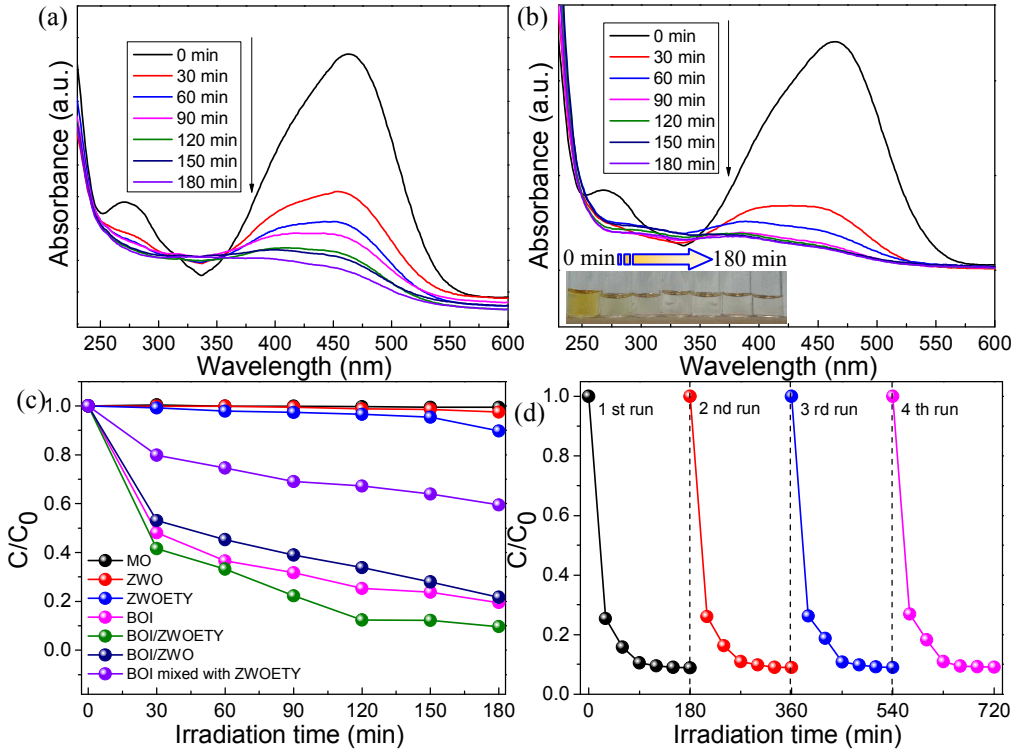

Fig. 5 Time-dependent absorption spectra of MO for (a) BOI and (b) BOI/ZWOETY under Vis-NIR ($\lambda \geq 400$ nm) light irradiation provided by a 1000 W high pressure mercury lamp (inset: the photographs of MO photodegradation over BOI/ZWOETY as the reaction time extended. (c) C/C_0 conversion plots of MO over pure ZWO, ZWOETY, BOI, BOI/ZWOETY, BOI/ZWO, and BOI-ZWOETY physical mixture under Vis-NIR ($\lambda \geq 400$ nm) light irradiation provided by a 1000 W high pressure mercury lamp. (d) Repeated photocatalytic degradation of MO over BOI/ZWOETY under Vis-NIR ($\lambda \geq 400$ nm) light irradiation provided by a 1000 W high pressure mercury lamp.

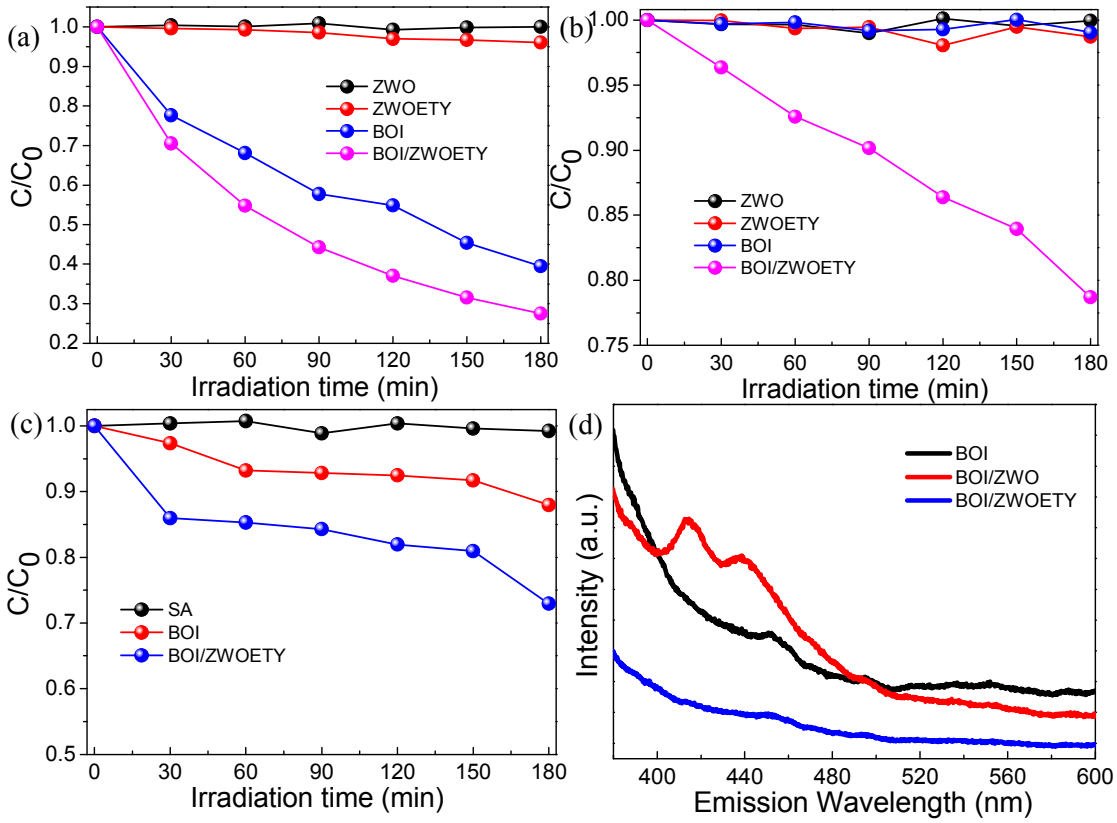

Fig. 6 (a) C/C_0 conversion plots of MO over the samples under Vis-NIR ($\lambda \geq 400$ nm) light irradiation provided by a 500 W Xe lamp. (b) C/C_0 conversion plots of MO over the samples under 980 nm NIR light irradiation (output current = 2.0 A). (c) C/C_0 conversion plots of SA over the samples under Vis-NIR ($\lambda \geq 400$ nm) light irradiation provided by a 1000 W high pressure mercury lamp. (d) PL emission spectra of pure BOI, BOI/ZWOETY, and BOI/ZWO excited at 343 nm at room temperature.

respectively. Thus, BOI/ZWOETY (BOI/10%ZWOETY) is chosen as the target for the following experiments. The band gap energies are calculated from the $(\alpha h\nu)^{1/2}$ versus photon energy ($h\nu$) plots (Fig. 3f) to be 3.44 eV (360 nm), 1.65 (752 nm) and 1.75 eV (709 nm) for ZWOETY, BOI and BOI/ZWOETY, respectively. Therefore, most of the visible light can be utilized by BOI, and only the limited UV light can be absorbed by ZWOETY.

Upconversion luminescence properties

The upconversion luminescence spectra of ZWOETY and BOI/ZWOETY under 980 nm NIR light excitation with the output currents increased from 1.0 A to 3.0 A are shown in Fig. 4a and c, respectively. Obviously, there exists remarked difference between the luminescence spectra profiles of ZWOETY and BOI/ZWOETY, and the emission intensities of ZWOETY are decreased largely after its combination with BOI, since that all the light emissions, including the red (658 nm, $^4F_{9/2} \rightarrow {}^4I_{15/2}$), green (526 and 550 nm, $^2H_{11/2}$, $^4S_{3/2} \rightarrow {}^4I_{15/2}$), blue (483 nm, $^1G_4 \rightarrow {}^3H_6$), and violet (410 nm, $^2H_{9/2} \rightarrow {}^4I_{15/2}$) light (Fig. 4b), can be harvested by BOI with the absorption edge of 709 nm. Meanwhile, in the BOI/ZWOETY composite, the 367 and 380 nm UV light produced by $^1D_2 \rightarrow {}^3H_6$ transitions of Tm^{3+} ions and $^4G_{11/2} \rightarrow {}^4I_{15/2}$ transitions of Er^{3+} ions (Fig. 4d), respectively, have been efficiently absorbed by BOI.

Photocatalytic performances

The decomposition of MO under Vis-NIR light irradiation is shown in Fig. 5, and the concentration (C/C_0) variations are quantified using the changed absorption peaks at 464 nm after the adsorption-desorption equilibrium. The absorbance of MO at 464 nm decreases greatly as the irradiation time increased over pure BOI (Fig. 5a) and BOI/ZWOETY (Fig. 5b), while BOI/ZWOETY displays the remarkable decolorization process (inset of Fig. 5b) with a removal rate of 91.12%, significantly higher than those of pure BOI (80.50%) and BOI/ZWO (78.34%) (Fig. 5c). The stability of BOI/ZWOETY is evaluated by the repeated experiments, and there is no obvious loss in photocatalytic activities after four times (Fig. 5d), indicating the good stability and the compact interface combination for BOI/ZWOETY. Meanwhile, BOI-ZWOETY physical mixture exhibits much lower removal rate (40.55%) compared to that of BOI/ZWOETY, since there are few contact interfaces between BOI and ZWOETY particles. In addition, pure ZWO has no photocatalytic activity under Vis-NIR light irradiation. Although the semiconductor upconversion agent of ZWOETY possesses strong upconversion luminescence and lower PL emission intensity compared to that of pure ZWO (Fig. S4†), due to its limited absorption edge of 360 nm (Fig. 3f), only a small removal rate of 10.22% is obtained for ZWOETY.

The high photocatalytic activities of BOI/ZWOETY are contributed by both the visible and NIR light. Benefit from the n-type semiconductor upconversion agent of ZWOETY, BOI/ZWOETY possesses the p-n heterostructure, which provides the lower PL emission intensity (Fig. 6d) and the better electron-hole separation compared to pure BOI and

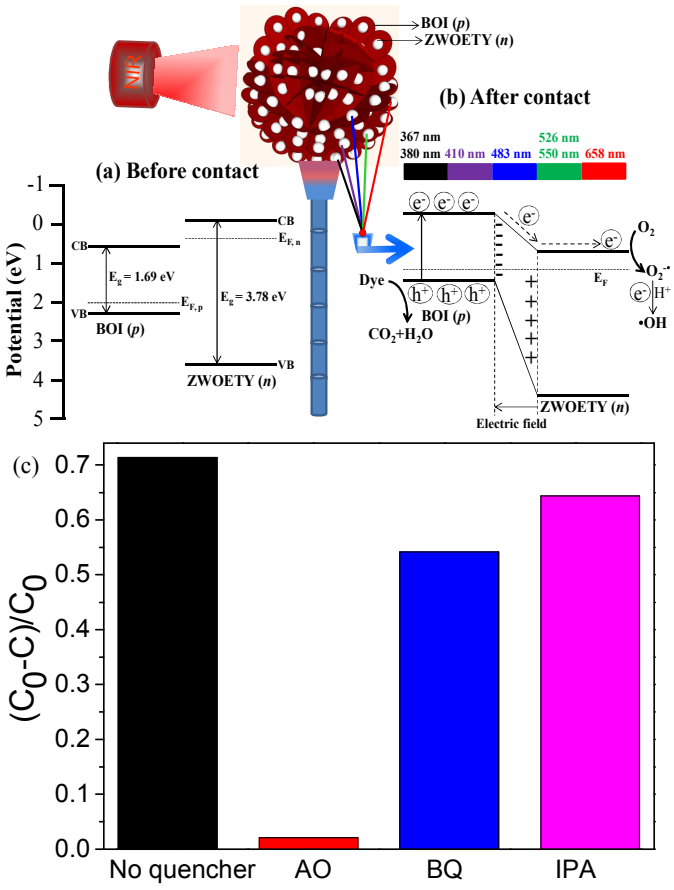

Fig. 7 (a) Schematic diagrams for energy bands of pure BOI and ZWOETY, and (b) the photocatalytic mechanism of the formed BOI/ZWOETY p-n heterostructure. (c) The effects of different scavengers (AO, BQ, and IPA) on the photocatalytic degradation of MO over BOI/ZWOETY with 30 min Vis-NIR light irradiation ($\lambda \geq 400$ nm) provided by a 1000 W high pressure mercury lamp.

BOI/ZWO. Thus, a higher Vis-NIR light driven degradation rate of 72.48% is obtained over BOI/ZWOETY under a 500 W Xe lamp irradiation, and only 3.93% and 60.48% are present in ZWOETY and pure BOI (Fig. 6a). Moreover, in comparison to the neglected degradation rates of ZWO, ZWOETY, and pure BOI with the 980 nm NIR light irradiation, BOI/ZWOETY still has a higher removal rate of 21.30% (Fig. 6b). This is attributed that all the red (658 nm), green (526 and 550 nm), blue (483 nm), violet (410 nm), and UV (367 and 380 nm) light emissions upconverted by ZWOETY can be absorbed by BOI for photocatalysis. Based on the above beneficial effects, BOI/ZWOETY also presents better photocatalytic activity (27.06%) compared to pure BOI (12.06%) in degradation of SA under Vis-NIR light irradiation (Fig. 6c).

Photocatalytic mechanism

According to Mulliken electronegativity theory,[17] the potentials of the conduction band (CB) and valance band (VB) edges for BOI and ZWOETY can be calculated using the following equation: $E_{VB} = X - E^e + 0.5\ E_g$, where X is the absolute electronegativity of the semiconductors, which is expressed as the geometric mean of the absolute electronegativity of the constituent atoms, with the values of 5.94 and 6.23 eV for BOI and ZWOETY,[13] respectively; E^e is the energy of free electrons on the hydrogen scale (4.5 eV); E_g is the band gap of the semiconductor. The CB can be determined by $E_{CB} = E_{VB} - E_g$. Thus, the E_{VB} values of BOI and ZWOETY are calculated to be 2.29 and 3.62 eV, respectively, and the corresponding E_{CB} values are 0.595 and -0.04 eV for BOI and ZWOETY, respectively (Fig. 7a). The Fermi energy level of the p-type BOI is close to the VB, and that of the n-type ZWOETY is close to the CB.[23,24] Because of the smaller work function of ZWOETY, the Fermi energy level of BOI is lower than that of ZWOETY.[13] Thus, when BOI and ZWOETY are in contact, the equilibration Fermi level (E_F) between two sides can be formed (Fig. 7b), and an internal electric field at the interface is built to enhance the photogenerated electron-hole pair separation under visible and NIR light irradiation.

The active electrons (e^-) can be scavenged by the surface adsorbed O_2 to yield $O_2^{\bullet-}$ radicals, which contribute for the MO degradation.[25] As shown in Fig. S5a†, the UV-vis absorption spectra of NBT at 259 nm decrease as the irradiation time extended under Vis-NIR light irradiation, while the amount of the $O_2^{\bullet-}$ radicals generated is not significant. Meanwhile, the •OH radicals are also detected and shown in Fig. S5b†, and the PL intensities of 2-hydroxyterephthalic acid at 423 nm are increased slightly. It was reported that the small content of •OH radicals over BOI are produced through the reactions between $O_2^{\bullet-}$ and H^+, rather than the generation from holes and the surface adsorbed H_2O,[15] owing that the standard redox potential of Bi(v)/Bi(Ⅲ) (+1.59 V) is more negative compared to that of •OH/$^-$OH (+1.99 V).[26] Considering the high degradation rates and the small amount of $O_2^{\bullet-}$ and •OH radicals, the main contributed active species should be attributed to the photogenerated holes (h^+). Based on the active species trapping results (Fig. 7b and S6†), it can be found that the MO and SA degradations are completely suppressed by AO, meaning that h^+ is more important than $O_2^{\bullet-}$ and •OH radicals, which can directly decompose organic pollutants, and it is consistent with the results found in other BOI based photocatalysts.[18] On the other hand, unlike the previous reported BOI photocatalysts,[15] BOI/ZWOETY possesses the advantage of NIR light driven photocatalytic activity, and will open up wide applications for sunlight utilization in environmental remediation.

Conclusions

A novel NIR photocatalyst of BOI/ZWOETY is prepared by a simple chemical precipitation method. Coupled with the n-type semiconductor upconversion agent of ZWOETY, the NIR light can be converted to the red (658 nm), green (526 and 550 nm), blue (483 nm), violet (410 nm), and UV light (367 and 380 nm), which are able to excite BOI to increase the photocatalytic activity. The formed p-n heterostructure between BOI and ZWOETY can also enhance the electron-hole pair separation in the BOI/ZWOETY composite. Under Vis-NIR light irradiation, BOI/ZWOETY exhibits higher degradation rates of MO and SA compared to those of ZWO, ZWOETY, pure BOI, and BOI/ZWO, which are contributed by both the upconversion and heterostructure advantages provided by ZWOETY.

Acknowledgements

This work was supported by Program of Shanghai Subject Chief Scientist (12XD1403000), Key Project of the National Research Program of China (2014BAL02B03), National Natural Science Foundation of China (no. 41173108), and

Shanghai Rising-Star Program (14QA1402400). We also thank Shanghai Tongji Gao Tingyao Environmental Science & Technology Development Foundation.

Notes and references

[a] School of Environmental Science and Engineering, Shanghai Jiao Tong University, 800 Dongchuan Road, Shanghai, 200240, P. R. China. Fax: +86 21 54743710; Tel: +86 21 54743710; E-mail: nwzhu@sjtu.edu.cn
[b] Daqing oilfield engineering Co., Ltd, CNPC, Daqing, Heilongjiang, 163712, P. R. China

† Electronic Supplementary Information (ESI) available: XRD patterns and UV-Vis-NIR diffuse reflectance spectra of other BOI/ZWOETY composites. Photocatalytic degradation results of salicylic acid under Vis-NIR light irradiation. See DOI: 10.1039/b000000x/

1 S. G. Kumar and L. G. Devi, *J. Phys. Chem. A*, 2011, **115**, 13211-13241.
2 R. A. He, S. W. Cao, P. Zhou and J. G. Yu, *Chin. J. Catal.*, 2014, **35**, 989-1007.
3 J. Zhang, J. G. Yu, Y. M. Zhang, Q. Li, and J. R. Gong, *Nano Lett.*, 2011, **11**, 4774-4779.
4 X. Y. Guo, W. Y. Song, C. F. Chen, W. H. Di and W. P. Qin, *Phys. Chem. Chem. Phys.*, 2013, **15**, 14681-14688.
5 Y. N. Tang, W. H. Di, X. S. Zhai, R. Y. Yang and W. P. Qin, *ACS Catal.*, 2013, **3**, 405-412.
6 S. Q. Huang, N. W. Zhu, Z. Y. Lou, L. Gu, C. Miao, H. P. Yuan and A. D. Shan, *Nanoscale*, 2014, **6**, 1362-1368.
7 S. Q. Huang, L. Gu, C. Miao, Z. Y. Lou, N. W. Zhu and H. P. Yuan, A. D. Shan, *J. Mater. Chem. A*, 2013, **1**, 7874-7879.
8 C. H. Li, F. Wang, J. Zhua and J. C. Yu, *Appl. Catal., B*, 2010, **100**, 433-439.
9 F. Wang and X. G. Liu, *Chem. Soc. Rev.*, 2009, **38**, 976-989.
10 J. Ungelenk, M. Speldrich, R. Dronskowski and C. Feldmann, *Solid State Sci.*, 2014, **31**, 75-80.
11 X. X. Luo and W. H. Cao, *J. Mater. Res.*, 2008, **23**, 2078-2083.
12 F. G. Yang, Z. Y. You and C. Y. Tu, *Laser Phys. Lett.*, 2012, **9**, 204-206.
13 P. Li, X. Zhao, C. J. Jia, H. G. Sun, Y. L. Li, L. M. Sun, X. F. Cheng, L. Liu and W. L. Fan, *J. Mater. Chem. A*, 2013, **1**, 3421-3429.
14 D. Q. He, L. L. Wang, D. D. Xu, J. L. Zhai, D. J. Wang and T. F. Xie, *ACS Appl. Mater. Interfaces*, 2011, **3**, 3167-3171.
15 L. Q. Ye, Y. R. Su, X. L. Jin, H. Q. Xie and C. Zhang, *Environ. Sci.: Nano*, 2014, **1**, 90-112.
16 L. Chen, R. Huang, M. Xiong, Q. Yuan, J. He, J. Jia, M. Y. Yao, S. L. Luo, C. T. Au and S. F. Yin, *Inorg. Chem.*, 2013, **52**, 11118-11125.
17 J. Jiang, X. Zhang, P. B. Sun and L. Z. Zhang, *J. Phys. Chem. C*, 2011, **115**, 20555-20564.
18 L. Q. Ye, X. D. Liu, Q. Zhao, H. Q. Xie and L. Zan, *J. Mater. Chem. A*, 2013, **1**, 8978-8983.
19 N. Zhang, S. Q. Liu, X. Z. Fu and Y. J. Xu, *J. Phys. Chem. C*, 2011, **115**, 9136-9145.
20 L. Q. Ye, J. Y. Liu, Z. Jiang, T. Y. Peng and L. Zan, *Nanoscale*, 2013, **5**, 9391-9396.
21 H. B. Fu, C. S. Pan, W. Q. Yao and Y. F. Zhu, *J. Phys. Chem. B*, 2005, **109**, 22432-22439.
22 Y. G. Su, L. M. Peng, J. W. Guo, S. S. Huang, L. Lv and X. J. Wang, *J. Phys. Chem. C*, 2014, **118**, 10728-10739.
23 H. T. Yu, S. Chen, X. Quan, H. M. Zhao and Y. B. Zhang, *Appl. Catal., B*, 2009, **90**, 242-248
24 L. Chen, S. F. Yin, S. L. Luo, R. Huang, Q. Zhang, T. Hong and P. C. Au, *Ind. Eng. Chem. Res.*, 2012, **51**, 6760-6768.
25 C. C. Chen, W. H. Ma and J. C. Zhao, *Chem. Soc. Rev.*, 2010, **39**, 4206-4219.
26 H. Fu, C. Pan, W. Yao and Y. Zhu, *J. Phys. Chem. B*, 2005, **109**, 22432-22439.

Graphical Abstract

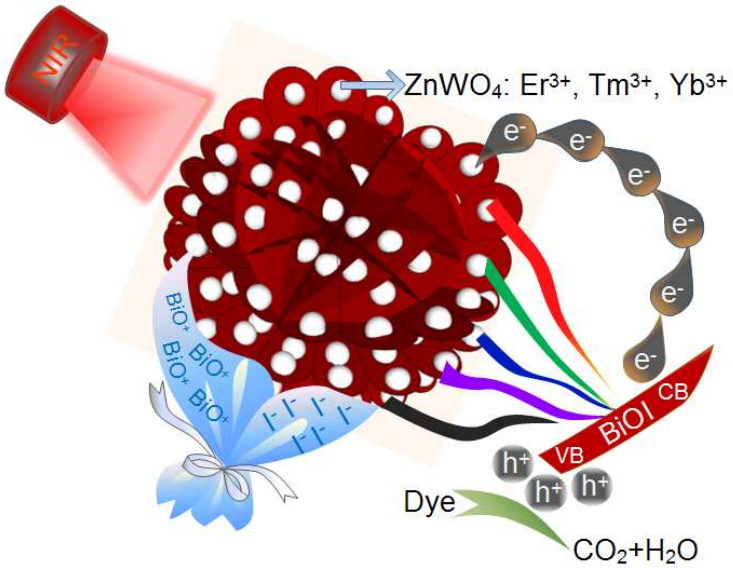

An efficient semiconductor upconversion agent of $ZnWO_4$: Er^{3+}, Tm^{3+}, Yb^{3+} (ZWOETY) was applied to synthesize the BiOI/ZWOETY composite with p-n heterostructure.